ELSEVIER

Marine Geology 229 (2006) 1 – 14

MARINE GEOLOGY
INTERNATIONAL JOURNAL OF MARINE GEOLOGY, GEOCHEMISTRY AND GEOPHYSICS

www.elsevier.com/locate/margeo

Estimating mud expulsion rates from temperature measurements on Håkon Mosby Mud Volcano, SW Barents Sea

N. Kaul [a,*], J.-P. Foucher [b], M. Heesemann [a]

[a] *Universität Bremen, Geowissenschaften, Klagenfurter Strasse, 28359 Bremen, Germany*
[b] *IFREMER, BP70, 29280 Plouzane, France*

Received 10 May 2005; received in revised form 2 February 2006; accepted 9 February 2006

Abstract

The Håkon Mosby Mud Volcano (HMMV), located on the Norwegian–Barents–Svalbard continental margin in 1250 m water depth, has been identified and described as a structure caused by upward transport of mud, pore water and gas [e.g. Eldholm, O., Sundvor, E., Vogt, P.R., Hjelstuen, B.O., Crane, K., Nilsen, A.K., Gladczenko, T.P., 1999. SW Barents Sea continental margin heat flow and Håkon Mosby Volcano. Geo-Marine Letters 19, 29–37]. During *RV Polarstern* expedition ARK XIX/3b in 2003, an integrated study took place to investigate the detailed morphology, biology, chemistry and geophysical aspects of HMMV [Klages, M., Thiede, J., Foucher, J.-P., 2004. The Expeditions ARK XIX 3a, 3b and 3c, Berichte zur Polarforschung, 488.]. In this paper, we describe a detailed survey involving more than 100 temperature gradient measurements in order to reveal the temperature structure of HMMV. Values of apparent heat flow up to 3000 mW/m^2 and absolute temperatures up to 25.8 °C have been detected. These enormously high heat flux values do not reflect deep-seated thermal gradients but are a result of surface mud flows. The occurrence and abundance of mud flows varies in different areas within the HMMV inner crater. A combination of very shallow, ROV-derived temperature measurements, a large number of intermediate depth temperature gradients and nine deep penetrating gravity corers allows us to reconstruct the history of activity of HMMV. Modeling of the observed temperature gradients indicates vigorous activity with very recent mud flows. Furthermore, the supply of energy and material from the HMMV is estimated to have an annual mass volume of ~15,000 m^3. From the thermal corona of HMMV and the observed horizontal heat flux, it is possible to deduce that the long term temperature of the mud pond is stable at a temperature approximately similar to the recent maximum temperature of 25 °C.

Keywords: seafloor hydrothermal system; mud volcano; heat flow; convection; SW Barents Sea

1. Introduction

During the multi-discipline *R/V Polarstern* cruise ARK XIX/3b (27 June 2003 to 19 July 2003), investigations of Håkon Mosby Mud Volcano (HMMV) were carried out to better understand the thermal structure of this 1 km wide pond. A review of heat flow measurements and the thermal field in the Norwegian–Greenland Sea associated with HMMV

* Corresponding author. Universität Bremen, FB5, PO box 330440, 28334 Bremen, Germany. Tel.: +49 421 218 7162; fax: +49 421 218 7163.
E-mail addresses: nkaul@uni-bremen.de (N. Kaul), Jean.Paul.Foucher@ifremer.fr (J.-P. Foucher), heesema@uni-bremen.de (M. Heesemann).

0025-3227/$ - see front matter © 2006 Elsevier B.V. All rights reserved.
doi:10.1016/j.margeo.2006.02.004

was given by Eldholm et al. (1999), while the thermal evolution of the Svalbard Margin was investigated systematically by Crane et al. (1988) (Fig. 1). These studies reveal a regional background heat flow of 53–75 mW/m^2 with only slight excursions up to 122 mW/m^2 observed when crossing the Senja Fracture Zone (SFZ) (Sundvor et al., 2000). Heat flow values decrease slightly from the Lofoten Basin in the West (water depth of 2800 m) to the SW Barents Sea in the East (water depth of only 500 m). Interpretation of seismic data (Hjelstuen et al., 1999) shows that as water depth decreases, the section of pre-glacial and glacial sediments on top of oceanic crust increases from ~3 km to a maximum of ~6 km. The HMMV is situated near the maximum sediment thickness within the basin and is underlain by 3 km of glacial sediment plus 3.2 km of pre-glacial sequences. Ties to commercial wells indicate an age of 2.3 Ma for the base of the glacial unit (Fiedler and Faleide, 1996), implying an extremely high sedimentation rate of 135 cm/1000 yr for the last 2.3 Ma. Based on magnetic anomalies, an age of 33–37 Ma is estimated for the underlying oceanic crust (Hjelstuen et al., 1999). Calculating a background heat flow according to the general model of Parsons and Sclater (1977) predicts a value of ~80 mW/m^2.

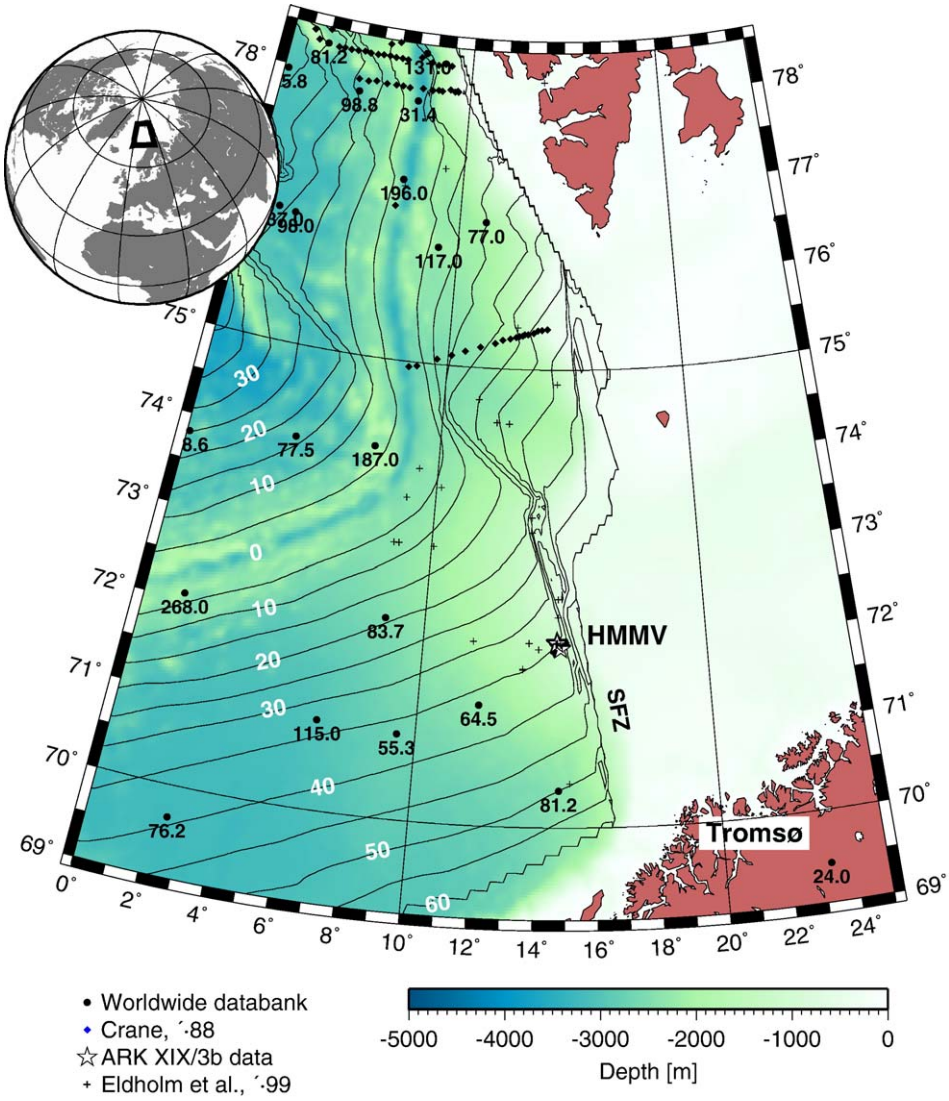

Fig. 1. Working area in the southwest Barents Sea and regional heat flow determinations. Håkon Mosby Mud Volcano (HMMV) is situated at a scarp on the flank of the Barents–Svalbard continental margin. Bathymetry data from ETOPO2 (NGDC, 2004) dataset allows to identify this depression. Age of oceanic crust is taken from Müller (1997). HMMV area is closely sampled with temperature measurements.

Eldholm (1999) reported unusually high heat flow values, up to 1000 mW/m^2 at HMMV that indicate convective heat transport. At the same time, optical imagery observed features attributed to gas or fluid expulsion (Vogt et al., 1997). Therefore, detailed thermal investigations were planned along with numerous geological work on methane gas and gas hydrate occurrences at HMMV. This structure has been inferred as an active mud volcano due to outflow channels, observed by side scan sonar observations (Vogt et al., 1999). Taking the terminology for mud structures (i.e. Camerlenghi et al., 1992; Cita et al., 1994; Camerlenghi et al., 1995; Kopf, 2002), the structure is a mud pie (flank slope <5°) rather than a volcano, signifying production of low viscosity mud. Gas hydrates have been recovered during coring (Ginsburg et al., 1999). As a consequence, we expect a thermal field, which is heavily affected by transient effects and mass convection. Under these circumstances, it would be misleading to use the term heat flow determinations, as this requires at least a quasi-steady-state situation for a reasonable long time period. We rather refer to temperature measurements and processes they describe.

2. Instrumentation

Three different tools were used to measure a large number of temperature gradients in the shallow (<1 m), intermediate (0–4 m) and "deep" (up to 16 m below seafloor (mbsf)) depth range. The lateral resolution varied from 50 m to some hundred meters, depending on the instrument used.

During this cruise, it was possible to take advantage of remotely operated vehicle (ROV) "Victor 6000" for shallow and closely spaced temperature measurements. During several dives, shallow seafloor temperature gradients at a spacing of 50 m were obtained. A temperature lance fitted with two Micrel THP type autonomous data loggers was used (Géli et al., 2001). These temperature loggers have a resolution of better than 1 mK at 20 °C and a capacity of ~25000 samples with data compression. The housing has a diameter of 28 mm and is rated at 600 bar. Two of these sensors were mounted 0.25 and 0.55 m below the top of a lance, which could be handled by the ROVs manipulator arm (Fig. 2). Penetration depth was controlled very accurately by "Victor 6000" so that we were confident to get an accurate temperature gradient for the uppermost decimeters below the mud line.

For the medium depth range between 0.8 and 4 m, a conventional heat flow probe for multipenetration stations was used. The Bremen heat probe is a violin bow instrument of Lister-type design and capable of 3.5 m penetration with 11 sensors distributed over a length of 3 m at a spacing of 0.3 m. Furthermore, this probe determines in-situ thermal conductivity at all 11 thermistor positions (Hyndman et al., 1979).

To extend "shallow" temperature measurements to greater depth, a gravity corer was equipped with autonomous temperature probes. Ten instruments of Micrel THP type (for specifications see above) were welded onto the core barrel at 0.88 or 1 m spacing. Six gravity corer stations gave reliable temperature measurements up to a maximum depth of 16 m. Three stations failed due to bent core barrels. We attribute this to rigid layers of gas hydrate located several meters below the seafloor, which could not be penetrated.

3. Thermal measurements

A total number of 98 successful temperature gradient determinations were achieved with the Bremen heat

Fig. 2. Mini-temperature lance equipped with two MICREL THP temperature sensors.

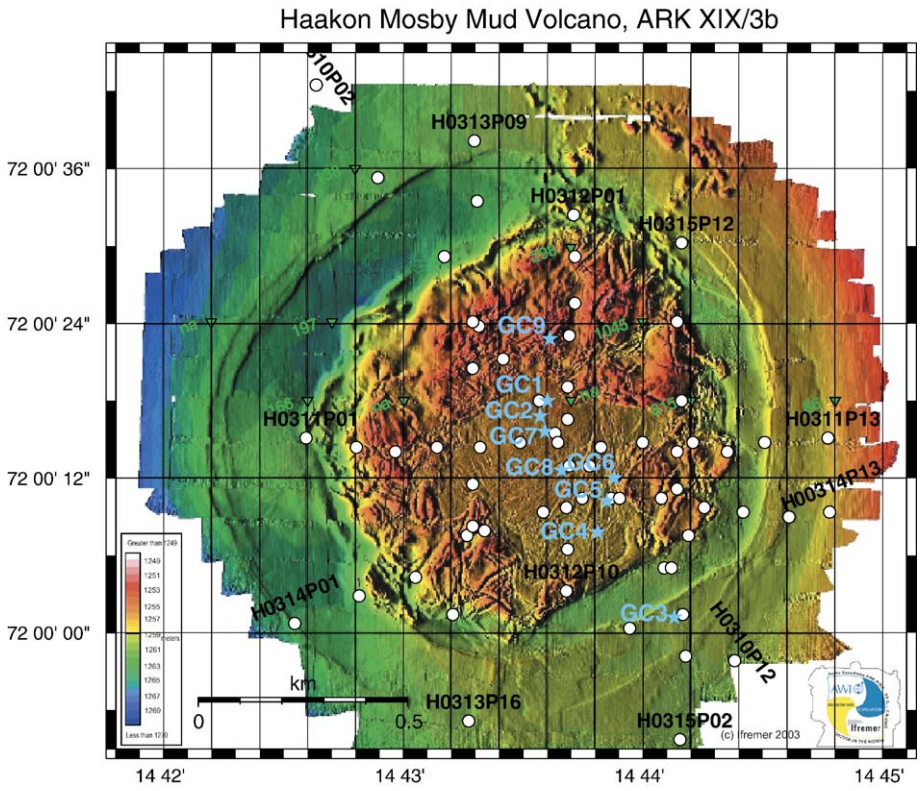

Fig. 3. High resolution bathymetry of Håkon Mosby Mud Volcano, produced by IFREMER, using deep towed multi-beam echo sounders, mounted beneath ROV "Victor 6000". Overlain are positions of heat flow sites (white dots) and gravity corers (blue stars). A regional classification is (i) outside the moat, (ii) the moat ring, (iii) a rough area north and west of the centre and (iv) a smooth area expanding from the centre southwards. (For interpretation of the references to colour in this figure legend, the reader is referred to the web version of this article.)

probe and an additional nine vertical profiles were made with a gravity corer, equipped with thermistors, plus two horizontal profiles of shallow temperature measurements with the mini-lance, operated with "Victor 6000". All measurements are concentrated on the HMMV crater, including its moat.

The survey across HMMV was planned for detailed investigation, so that distances between points in a given line are as short as 100 m across the center, and 200–300 m outside that region (Fig. 3). From the very first profile (H0310), we learned that temperature anomalies are very distinct and limited in extent. Therefore, survey lines were planned to make a grid with many crossings near the center of HMMV. Eldholm et al. (1999) showed that background heat flow values of 55–70 mW/m^2 are present at a distance of only a few kilometers from HMMV. Thus, we did not extend our profiles more than 10 km from the center. The seafloor conditions are very favorable for instrument penetration down to 4 mbsf. Fig. 3 shows the distribution of these measurements overlain on high resolution bathymetry. The bathymetric map is a result of a systematic survey by the deep flying ROV "Victor 6000".

Detailed surveys with the mini-lance were located at key sites, chosen from previous heat flow investigations or visual inspection by ROV "Victor 6000". Navigation of the ROV is relative to the surface vessel by means of a Posidonia™ acoustic transponder. True ground positions were accurate within ±30 m, deduced from the relocation of known features. Only few sites were positioned outside the crater, up to 10 km away, in order to acquire a regional reference for temperatures and gradients.

Due to a very soft seafloor consistency in the center of HMMV, we have to consider "over-penetration" for the heavy instruments, i.e. penetration is larger than the maximum length of the lance and thus poorly constrained. The total penetration has then to be estimated by the mud line on the deep sea cable and the extrapolation of the thermal gradient (Table 1).

Table 1
Interpolated temperatures at relative depths with respect to the uppermost sensor

	Longitude	Latitude	HF-name	*k*	T_0m	T_1m	T_2m	T_3m	Gradient (mK/m)	PS64/station
1	14.7064	72.0136	H0310P01	1.11*	−0.76	−0.7	−0.63	−0.56	67	PS64/319-1
2	14.7115	72.0114	H0310P02	1.11	−0.75	−0.69	−0.52	−0.56	66	PS64/319-2
3	14.7167	72.0092	H0310P03	1.11	−0.69	−0.6	−0.52	−0.41	86	PS64/319-3
4	14.7201	72.0078	H0310P04	1.40*	−0.48	−0.31	−0.05	0.15	240	PS64/319-4
5	14.7235	72.0063	H0310P05	1.08*	−0.5	2	3.5	5.0	2740	PS64/319-5
6	14.7252	72.0056	H0310P06	1.08	5	5.5	8	10.5	2430	PS64/319-6
7	14.727	72.0049	H0310P07	1.08	24.5	26.0	25.4	25.2	−98	PS64/319-7
8	14.7287	72.0042	H0310P08	1.02*	11.5	12	14.5	17	2500	PS64/319-8
9	14.7304	72.0034	H0310P09	1.00*	4.5	6.5	8.4	10.5	2050	PS64/319-9
10	14.7321	72.0027	H0310P10	0.96*	7	9	11	13.3	2010	PS64/319-10
11	14.7355	72.0012	H0310P11	1.27*	−0.68	−0.59	−0.5	−0.41	90	PS64/319-11
12	14.7406	71.9991	H0310P12	1.19*	−0.78	−0.71	−0.64	−0.62	70	PS64/319-12
13	14.7458	71.9969	H0310P13	1.13*	−0.8	−0.74	−0.67	−0.61	62	PS64/319-13
14	14.7492	71.9954	H0310P14	1.11*	−0.8	−0.74	−0.68	−0.62	61	PS64/319-14
15	14.7528	71.9933	H0310P15	1.12*	−0.8	−0.74	−0.68	−0.62	60	PS64/319-15
16	14.7615	71.9893	H0310P16	1.12*	−0.81	−0.75	−0.69	−0.64	57	PS64/319-16
17	14.7112	72.0042	H0311P01	1.00	−0.8	−0.58	−0.42	−0.27	153	PS64/333-1
18	14.7141	72.0042	H0311P02	1.03*	−0.51	−0.1	0.3	0.8	433	PS64/333-2
19	14.717	72.0042	H0311P03	1.12*	0.5	1.4	2.3	3.1	936	PS64/333-3
20	14.7199	72.0042	H0311P04	1.18*	1.2	2.8	4.5	6.2	1760	PS64/333-4
21	14.7228	72.0042	H0311P05	1.00	23	23.8	24.2	24.6	402	PS64/333-5
22	14.7257	72.0042	H0311P06	1.00	16	18	20	22.5	2000	PS64/333-6
23	14.7288	72.0042	H0311P07	1.00	13.6	13.8	14.1	14.4	325	PS64/333-7
24	14.7316	72.0042	H0311P08	0.69*	10.1	11.8	13.4	15	1590	PS64/333-8
25	14.7345	72.0042	H0311P09	1.00	8.9	10	11	12	1070	PS64/333-9
26	14.7374	72.0042	H0311P10	1.15*	−0.2	0.3	0.9	1.5	564	PS64/333-10
27	14.7403	72.0042	H0311P11	1.00	−0.6	−0.45	−0.3	−0.17	138	PS64/333-11
28	14.7432	72.0042	H0311P12	1.34*	−0.72	−0.64	−0.56	−0.5	72	PS64/333-12
29	14.7461	72.0042	H0311P13	1.16*	−0.75	−0.68	−0.6	−0.56	75	PS64/333-13
30	14.7287	72.0087	H0312P01	1.16*	−0.5	−0.3	−0.06	0.15	229	PS64/333-14
31	14.7287	72.0078	H0312P02	1.11*	−0.2	0.5	1.2	1.9	708	PS64/333-15
32	14.7287	72.0069	H0312P03	1.22*	−0.8	−0.2	0.3	1.0	?	PS64/333-16
33	14.7287	72.006	H0312P04	1.7*	−0.8	−0.6	0.2	0.9	834	PS64/333-17
34	14.7287	72.0051	H0312P05	0.73*	4.5	6.2	8.3	10.1	1990	PS64/333-18
35	14.7287	72.0043	H0312P06	1.19*	2.5	4.4	6.2	8	1870	PS64/333-19
36	14.7287	72.0033	H0312P07	1.10	10	12	14.2	16.5	2140	PS64/333-20
37	14.7287	72.0024	H0312P08	0.99*	4	6	8	10	2090	PS64/333-21
38	14.7287	72.0015	H0312P09	1.13*	5	7	8.6	10.8	1910	PS64/333-22
39	14.7287	72.0006	H0312P10	1.11*	−0.5	−0.2	0.1	0.39	275	PS64/333-23
40	14.7217	72.0255	H0313P01	1.1	−0.79	−0.73	−0.68	−0.62	53	PS64/343-1
41	14.7216	72.0237	H0313P02	1.1	−0.78	−0.73	−0.67	−0.62	55	PS64/343-2
42	14.7215	72.0219	H0313P03	1.09*	−0.78	−0.73	−0.66	−0.61	58	PS64/343-3
43	14.7213	72.0201	H0313P04	1.1	−0.77	−0.72	−0.66	−0.6	59	PS64/343-4
44	14.7212	72.0183	H0313P05	1.09*	−0.78	−0.72	−0.66	−0.6	59	PS64/343-5
45	14.7211	72.0165	H0313P06	1.1	−0.77	−0.72	−0.65	−0.59	61	PS64/343-6
46	14.721	72.0147	H0313P07	1.13*	−0.75	−0.69	−0.62	−0.55	66	PS64/343-7
47	14.721	72.0129	H0313P08	1.15*	−0.72	−0.65	−0.59	−0.51	71	PS64/343-8
48	14.7209	72.0111	H0313P09	1.1	−0.7	−0.63	−0.56	−0.49	73	PS64/343-9
49	14.7208	72.0093	H0313P10	1.1	−0.65	−0.57	−0.48	−0.39	89	PS64/343-10
50	14.7206	72.0067	H0313P11	1.10*	−0.3	0.12	0.52	0.9	418	PS64/343-11
51	14.7205	72.0057	H0313P12	1.06*	−0.8	0	2	4	2090	PS64/343-12
52	14.7204	72.0033	H0313P13	1.1	17	19.5	22.3	25	2920	PS64/343-13
53	14.7203	72.0021	H0313P14	1.1	7	10	13.5	17	2820	PS64/343-14
54	14.7202	72.0003	H0313P15	1.22*	−0.6	−0.2	0.3	0.8	479	PS64/343-15
55	14.7201	71.9985	H0313P16	1.30*	−0.73	−0.66	−0.60	−0.52	69	PS64/343-16
56	14.72	71.9967	H0313P17	1.32*	−0.75	−0.69	−0.63	−0.56	59	PS64/343-17
57	14.7199	71.9949	H0313P18	1.1	−0.76	−0.71	−0.65	−0.58	60	PS64/343-18

(continued on next page)

Table 1 (*continued*)

	Longitude	Latitude	HF-name	*k*	T_0m	T_1m	T_2m	T_3m	Gradient (mK/m)	PS64/station
58	14.7198	71.9931	H0313P19	1.1	−0.77	−0.71	−0.65	−0.59	58	PS64/343-19
59	14.7142	72.0013	H0314P01	1.34*	−0.74	−0.66	−0.6	−0.54	59	PS64/361-1
60	14.7088	72.0007	H0314P02	1.1	−0.6	−0.5	−0.41	−0.31	93	PS64/361-2
61	14.717	72.0016	H0314P03	1.22*	−0.6	−0.45	−0.1	0.25	290	PS64/361-3
62	14.7197	72.0019	H0314P04	1.1	9	10.5	11.8	13	1310	PS64/361-4
63	14.7224	72.0022	H0314P05	1.21*	−0.51	−0.1	0.56	na	930	PS64/361-5
64	14.7252	72.0025	H0314P06	0.95*	13	14.4	15.8	17.1	1440	PS64/361-6
65	14.7279	72.0028	H0314P07	1.17*	8	10	11	11.5	1150	PS64/361-7
66	14.7308	72.0028	H0314P08	1.30*	7.9	9.3	10.9	13.3	1540	PS64/361-8
67	14.7337	72.0028	H0314P09	1.09*	−0.2	0.4	1.1	1.55	688	PS64/361-9
68	14.7366	72.0028	H0314P10	1.13*	−0.7	0.0	0.7	na	677	PS64/361-10
69	14.7396	72.0028	H0314P11	1.23*	−0.6	−0.47	−0.33	−0.2	127	PS64/361-11
70	14.7425	72.0028	H0314P12	1.30*	−0.7	−0.63	−0.56	−0.5	68	PS64/361-12
71	14.7454	72.0028	H0314P13	1.22*	−0.72	−0.65	−0.57	−0.51	70	PS64/361-13
72	14.7512	72.0028	H0314P14	1.10*	−0.76	−0.7	−0.63	−0.56	65	PS64/361-14
73	14.7348	71.9964	H0315P01	1.16*	−0.74	−0.67	−0.61	−0.55	65	PS64/361-15
74	14.7348	71.9982	H0315P02	1.25*	−0.74	−0.66	−0.60	−0.54	65	PS64/361-16
75	14.7348	72	H0315P03	1.34*	−0.71	−0.65	−0.59	−0.53	63	PS64/361-17
76	14.7348	72.0009	H0315P04	1.15*	−0.71	−0.64	−0.56	−0.49	78	PS64/361-18
77	14.7348	72.0018	H0315P05	1.27*	−0.6	−0.49	−0.36	−0.25	123	PS64/361-19
78	14.7348	72.0027	H0315P06	1.23*	−0.6	−0.2	0.3	0.8	480	PS64/361-20
79	14.7348	72.0036	H0315P07	1.20*	−0.3	0.6	0.9	na	918	PS64/361-21
80	14.7348	72.0045	H0315P08	1.14*	0.2	1.0	1.8	2.7	836	PS64/361-22
81	14.7348	72.0054	H0315P09	1.1	0.0	0.6	1.4	2.2	756	PS64/361-23
82	14.7359	72.0059	H0315P10	na	na	na	na	na	na	PS64/361-24
83	14.7348	72.0072	H0315P11	1.1	−0.2	0.4	1.0	1.6	637	PS64/361-25
84	14.7348	72.009	H0315P12	1.20*	−0.76	−0.6	−0.4	na	195	PS64/361-26
85	14.7317	72.0003	H0316P01	1.32*	−0.61	−0.4	−0.2	0.0	213	PS64/369-1
86	14.7479	71.9929	H0316P02	1.12*	−0.79	−0.74	−0.68	−0.62	58	PS64/369-2
87	14.7642	71.9854	H0316P03	1.1	−0.8	−0.75	−0.69	−0.64	54	PS64/369-3
88	14.7804	71.978	H0316P04	1.36*	−0.81	−0.77	−0.72	−0.68	42	PS64/369-4
89	14.7966	71.9705	H0316P05	1.1	−0.8	−0.75	−0.7	−0.65	50	PS64/369-5
90	14.8129	71.963	H0316P06	1.20*	−0.79	−0.74	−0.7	−0.66	43	PS64/369-6
91	14.8291	71.9556	H0316P07	1.1*	−0.77	−0.72	−0.67	−0.63	46	PS64/369-7
92	14.8453	71.9481	H0316P08	1.23*	−0.79	−0.75	−0.7	−0.65	47	PS64/369-8
93	13.4328	71.7018	H0317P01	1.21*	−0.79	−0.73	−0.68	−0.64	48	PS/64/389-1
94	13.4333	71.7000	H0317P02	1.21*	−0.78	−0.73	−0.68	−0.65	46	PS/64/389-1
95	13.4340	71.6982	H0317P03	1.1	−0.78	−0.73	−0.68	−0.65	42	PS/64/389-1
96	13.4353	71.6946	H0317P04	1.1	−0.8	−0.75	−0.7	−0.65	51	PS/64/389-1
97	13.4527	71.6589	H0317P05	1.14*	−0.83	−0.77	−0.72	−0.66	52	PS/64/389-2
98	13.4489	71.6571	H0317P06	1.15*	−0.81	−0.77	−0.72	−0.66	49	PS/64/389-2

Conductivity values *k** are calculated from measurements, others are spatially interpolated.

3.1. Surface measurements using a mini-lance

A closer look at the data from the mini-lance shows temperatures of 0 °C to +13 °C at 0.25 mbsf and +0.1 °C to +22 °C at 0.55 mbsf (Fig. 4). The maximum resulting temperature gradient within the uppermost half meter of the sediment is as high as 41,000 mK/m, assuming a bottom water temperature of −0.8 °C. This is far more than can be sustained by basal conductive heat flow, as this would lead to unrealistic high subseafloor temperatures, i.e. 1000 °C in only 25 m depth. This leads to the question: How deep do these high gradients reach?

3.2. Heat flow probe temperature determinations

Usage of the heat flow probe gives information on the temperature distribution down to ~3.5 mbsf at 92 locations within the crater and the immediate surrounding (up to 2 km distance from the center) and at six locations at a distance of ~45 km from the center. An example of one profile crossing HMMV from NW to SE is given in Fig. 5. The compilation of all data points in the vicinity of HMMV is given in Fig. 6. The singularity of the temperature distribution becomes evident from the smoothed *x*–*y*–*t* plot. The figure displays the temperature of the uppermost sensor

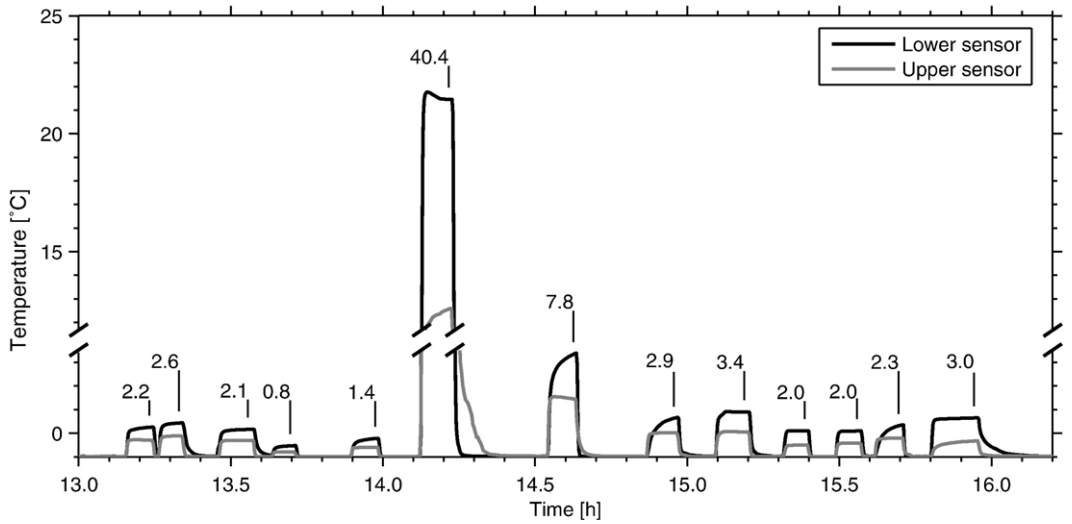

Fig. 4. Temperature measurements as time series of the two MICREL sensors, mounted onto a mini-lance. Sensor positions are 55 (black line) and 25 cm (grey line) below the top of the lance. The position of the maximum temperature coincides with the highest temperatures found with the Bremen heat probe. Numbers denote the vertical temperature gradient in °C/m.

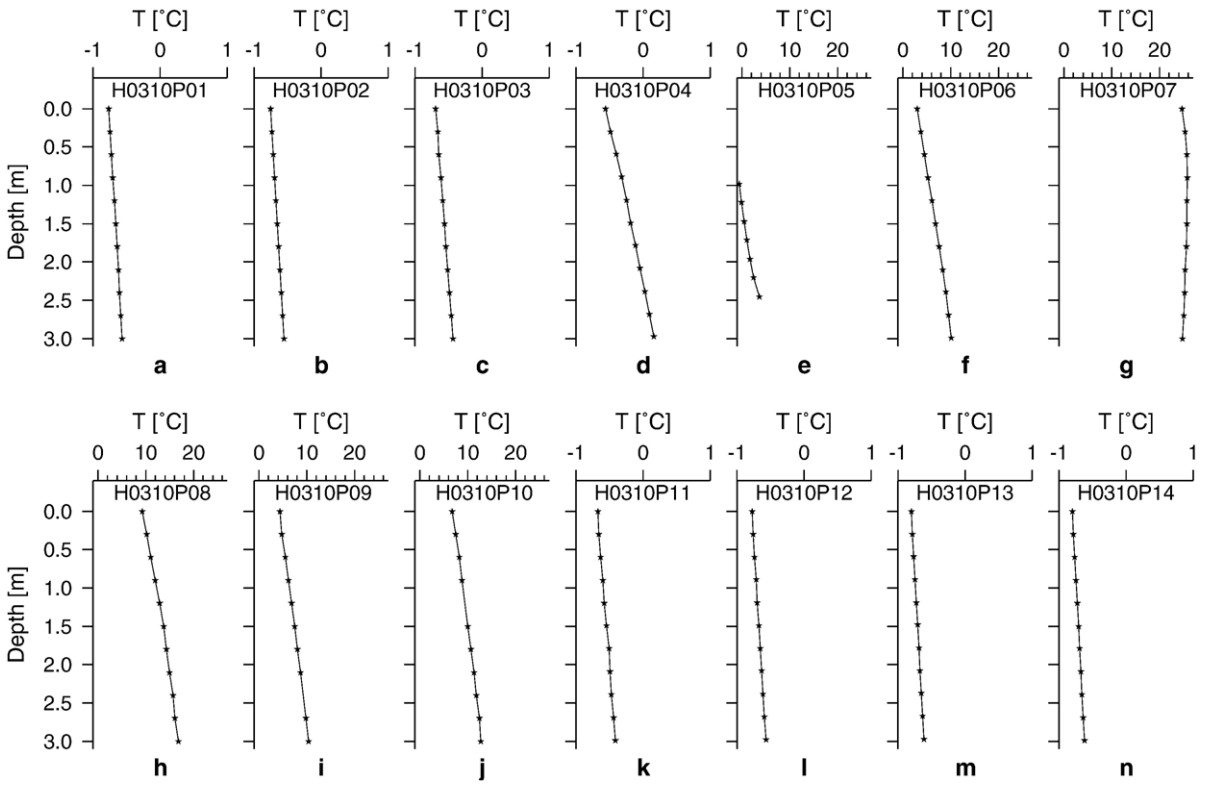

Fig. 5. Temperature–depth plots of station H0310, aligned in a NW–SE direction across the centre of HMMV. Temperature scales of figures e–j are compressed by a factor of 13 to accommodate for the higher temperatures within the central crater. At the very centre (H0310P07, g), high temperatures correlate with a low gradient.

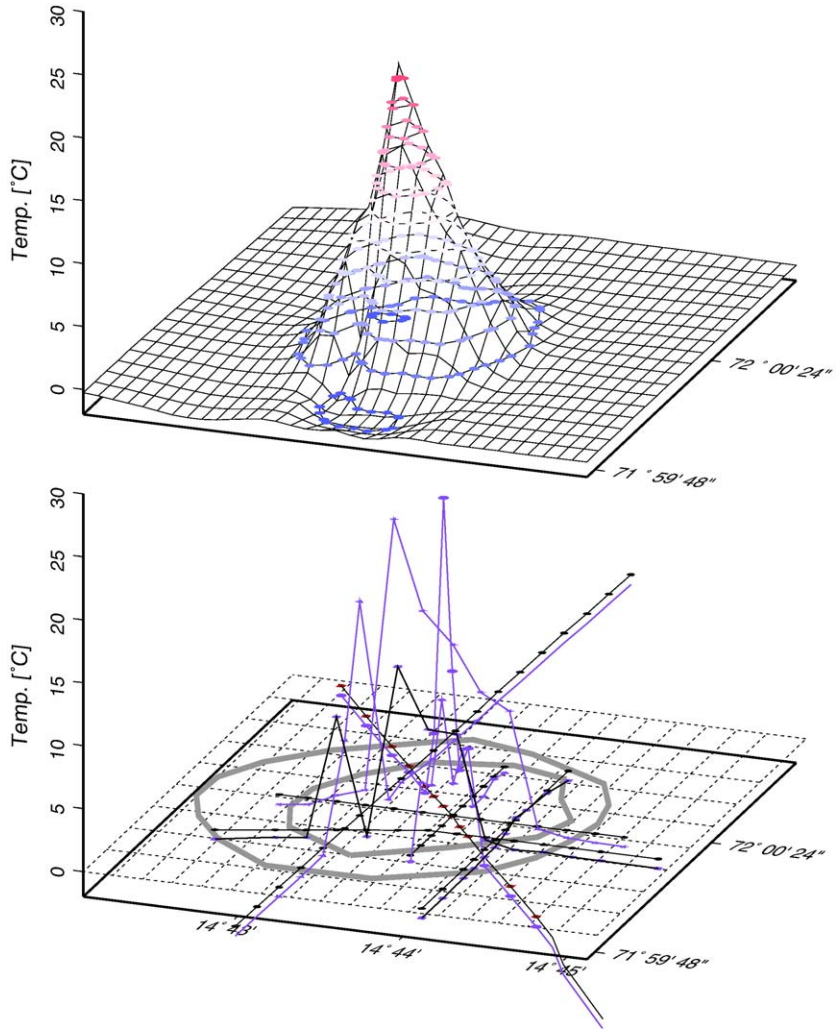

Fig. 6. Compilation of heat flow probe temperature data of the uppermost sensor (app. 0.7–0,8 mbsf) of all locations near HMMV. The upper part shows a smoothed version of the dataset, while the lower part displays the irregular distributed data points and their projections onto the base lines. Concentric circles indicate the position of inner and outer rim of HMMV.

(~0.8 mbsf) which shows the most pronounced special variation.

At a range of 1 km from the rim of the crater, we find seafloor temperatures as low as −0.8 °C immediately beneath the mud line, slightly increasing downward in the sediments, resulting in a vertical gradient of 55–65 mK/m within the uppermost 3 m. Thermal conductivity determinations, derived from in situ measurements, give values of 1.0–1.2 W/m K increasing downwards, with a mean value of ~1.1 W/m K. This results in heat flow values of 60–73 mW/m^2, a heat flow which has been found for the region within several hundred kilometers of the HMMV (Eldholm et al., 1999). Therefore, this station can be considered a reference station which is unaffected by the mud volcano.

A completely different observations is found at a location slightly NW of the geometrical center of the crater where an almost homogeneous temperature distribution at a temperature of +25 °C exists (Fig. 5g). A closer investigation of this site reveals that the temperature distribution has a clear maximum of 25.8 °C at 1–2 m depth, and decreasing temperatures both upward (24.7 °C) and downward (24.8 °C). This is the highest temperature encountered during this and all other published surveys of HMMV. The majority of measurements exhibit a more or less linear, positive gradient. Values range from ~60 mK/m to 2700 mK/m next to the center. Strong indications of convective heat transport within the pore space are indicated by curved gradients, observed occasionally. The curvature of

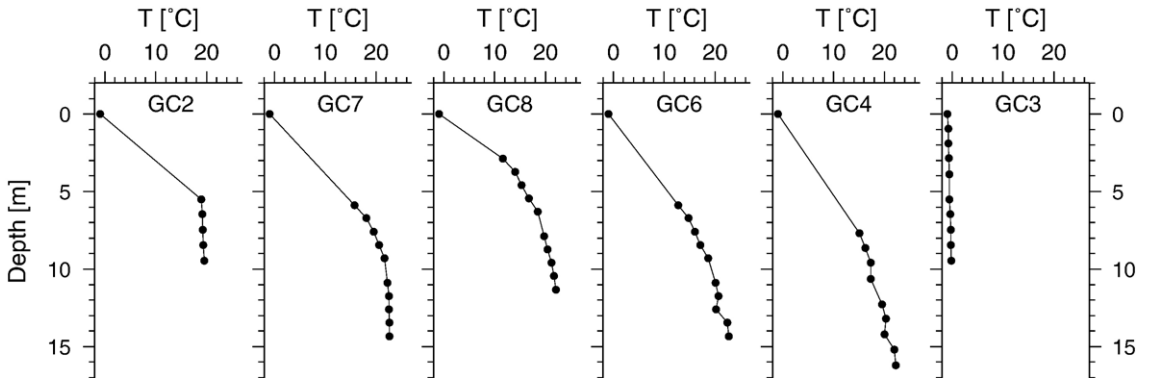

Fig. 7. Data from six successful gravity corers. (a) GC 2 located near the centre, (b–c) between centre and moat rim and (f) outside the moat rim. Temperature scale is identical −2 to +27 °C.

convex shaped thermal gradients was evaluated at eight locations, implying upward migration velocities of pore water of 0.3–6 m yr^{-1}. The distribution of fluid convection derived from chemical and thermal gradients is discussed in detail in de Beer et al. (2006). Looking at the distribution of temperatures, we find that a huge horizontal gradient exists. Taking values at 3–4 m depth, we find an overall horizontal gradient of 28.2 °C/km from a "normal" background gradient to the center (i.e. H0310P02–H0310P07, Fig. 5b–g). Across the moat rim of the crater, we find an enormous temperature difference of 13 °C over a horizontal distance of 200 m, indicating a gradient of 65 °C/km (H0310P10–H0310P11, Fig. 5j and k). Both vertical and horizontal gradients give evidence for a very active system, which is able to maintain such huge temperature gradients.

3.3. Gravity corers with attached temperature probes

Long gravity corers equipped with temperature probes allowed determination of deep temperature profiles within and outside the crater. Five sites are located near the center (GC 2, GC 4, GC 6, GC 7 and GC 8) and one site (GC 3) is positioned SE outside the rim (Fig. 3). Fig. 7a–f displays the temperature–depth correlations. Site GC 3 outside the crater shows a normal positive gradient of ~79 mK/m in good agreement with neighboring 3 m deep heat flow stations. At all other sites, gradients are not at all linear but tend to reach a maximum value in an asymptotic manner. A temperature of 23 °C is never exceeded at the depth range of the gravity corers (see Table 2). However, the asymptotic temperature increase is at its limit in two places (GC 2

Table 2
Temperature data of seven successful gravity corer measurements

Name	Latitude	Longitude											
GC1	72°0.30′N	14°43.60′E	No data										
GC2	72°0.28′N	14°43.57′E	0	5.52	6.46	7.46	8.46	9.45					[m]
			−0.8	18.95	19.15	19.22	19.4	19.59					[°C]
GC3	72°0.02′N	14°44.13′E	0	0.94	1.9	2.85	3.9	5.52	6.46	7.46	8.46	9.45	[m]
			−0.8	−0.78	−0.73	−0.64	−0.56	−0.51	−0.36	−0.29	−0.24	−0.19	[°C]
GC4	72°0.13′N	14°43.81′E	0	7.69	8.65	9.6	10.65	12.27	13.21	14.21	15.21	16.2	[m]
			−0.8	15.13	16.25	17.3	17.36	19.6	20.35	20	21.94	22.31	[°C]
GC5	72°0.17′N	14°43.85′E	No data										[m]
			–										[°C]
GC6	72°0.20′N	14°43.88′E	0	5.89	6.72	7.58	8.45	9.31	10.89	11.74	12.6	13.46	14.34	[m]
			−0.8	12.8	14.82	16.06	17.16	18.68	20.11	20.72	20.21	22.43	22.74	[°C]
GC7	72°0.20′N	14°43.88′E	0	5.89	6.72	7.58	8.45	9.31	10.89	11.74	12.6	13.46	14.34	[m]
			−0.8	15.8	18.1	19.55	20.61	21.72	22.31	22.59	22.55	22.68	22.64	[°C]
GC8	72°0.21′N	14°43.66′E	0	2.89	3.72	4.58	5.45	6.31	7.89	8.74	9.6	10.46	11.34	[m]
			−0.8	11.65	14.01	15.31	16.76	18.46	19.71	20.4	21.2	21.66	22.11	[°C]
GC9	72°0.38′N	14°43.61′E	0	0.72	1.58	2.45	3.31							[m]
			−0.8	0.35	0.67	1.87	3.13							[°C]

and GC 7), but not at sites GC 4, GC 6 and GC 8, suggesting even higher temperatures further below. It is noteworthy that the highest temperature of almost 26 °C has been found in the uppermost 4 mbsf and not in the deeper section.

4. Calculation of mud and fluid flow

From horizontal and vertical temperature distributions, we derived a model of eruptive mud expulsions from a single channel near the geometrical center of HMMV. As a temperature-difference of more than 25 °C to ambient environment is maintained within a considerable area of the crater, we have to suppose a heat supply at a rate, high enough to counteract conductive cooling. This leads to a number of questions: how often do eruptions occur? Can we determine the maximum temperature of a mud flow? Are estimates possible for the history of eruption in certain areas, deduced from temperature measurements?

As input dataset for modeling a singular mud flow, a combination of data at the central location is possible because individual positions of measurements are less than 50 m apart. We combine stations H0310P07 and GC 2 with data from the mini-lance in order to yield a 9.5 m long temperature profile with 18 data points. A bulge in the temperature profile (Fig. 8) is documented by shallow and medium deep sensors. Decreasing

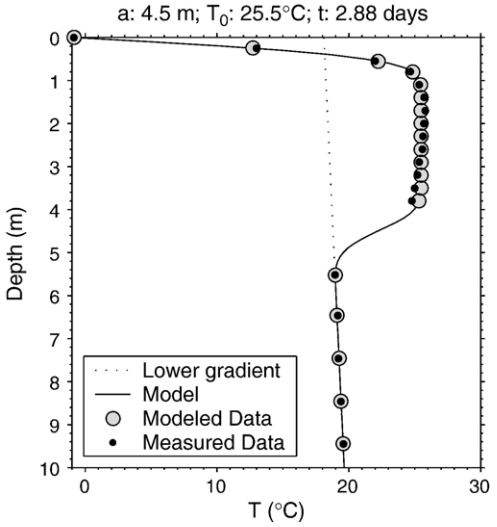

Fig. 8. A composite temperature profile from 0 to 10 mbsf. Data between 0 and 0.55 mbsf are from the mini-lance, 1–4 mbsf are from Bremen heat probe and 5–10 mbsf are from gravity corer #7. Small dots are data points and larger dots represent temperatures, modeled for one mud flow of 4.5 m thickness, extruded 3 days before at a temperature of 26 °C.

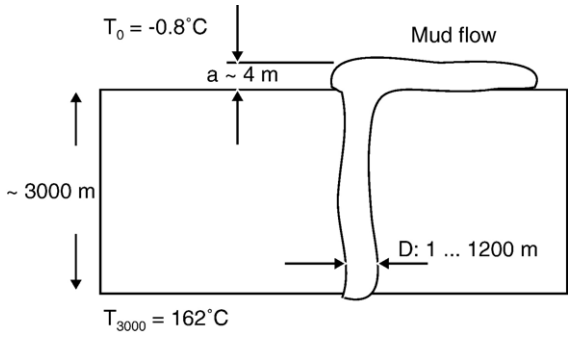

Fig. 9. Model parameters for a singular mud flow.

temperatures above 1 mbsf and below 4 mbsf indicate a layer thickness of warm material of ~4 m.

FEMLAB® 3.0a is used for finite-difference method numerical calculations. To start modeling, we hypothesize that warm mud is produced at the center of HMMV, producing distinctive mud flows (Fig. 9). The thickness (a) of this individual mud layer is estimated from the temperature maximum at penetration H0310P07 (Fig. 5g) to be 4 m. The expulsion temperature T_0 of this mud flow is suggested to be between 24 °C and 28 °C. The ambient seawater temperature above is around −0.8 °C. The lower boundary condition is a basal heat flow of 170 mW/m^2, deduced from the temperature gradient, found at site GC 2 (Table 3).

Fig. 8 shows the best fitting result with parameters T_0=25.5 °C and a time for temperature equalization of 2.9 days. Higher starting temperatures T_0 result in inadequate temperature distributions. Simulations with flow thicknesses of 2.5–5.5 m, and initial temperatures of 24.5–26.5 °C all give ages between 2.5 and 3.5 days for this specific mud flow. Thus, we are confident that we found a mud flow, younger than 3 days with a core temperature of 25.8 °C. Taking the above-mentioned mud flow as a singular effect, it would take 3.5 months to achieve equilibrium (99%) with its surroundings. The modeling is most sensitive to the uppermost temperature values and least sensitive to the basal heat flow; thus, even position uncertainties for site GC 2, which constrains the deeper part of the section, are not critical to the modeling result.

Table 3
Parameters for mud flow age calculation

Input	Output
T_0=26–28 °C	t=2.5–3.5 days
d=3.5–5.5 m	
Q_0=170 mW/m^2	
T_{Top}=−0.8 °C	

A second model hypothesis tries to elucidate the total volume of mud that has to be conveyed through the vertical conduit in order to feed a source of ~26 °C warm mud in a cold environment. We assume a single circular feeder channel of width D (Fig. 9), rooted at 3000 mbsf. The geometry of this model is derived from seismic data, published by Hjelstuen et al. (1999). Two seismic lines (D2-82 and 7200-77) give evidence that the conduit of HMMV originates at 2.5–3 km depth, that is within the 3.1 km thick glacial unit, deposited since Pliocene times. Our model starts at this depth as the most probable depth of origin and a temperature T (3000 m) of 162 °C representing the lower boundary condition. This temperature corresponds to a mean regional heat flow of 65 mW/m^2 at a thermal conductivity of 1.2 W/m K. The value for the thermal conductivity was chosen from our measurements outside HMMV (i.e. H0310P01) and extrapolated to greater depth. The upper boundary condition of the feeder channel is given by the outflow temperature of 26 °C. Densities of mud within the conduit and surrounding material are 1950 and 2000 kg/m^3, respectively. The specific thermal capacity of mud is taken as 1040 J/kg K. A number of simulations with varying diameters from 1 to 1200 m have been calculated in order to satisfy the thermal boundary conditions at the upper and lower end of the feeder channel (Table 4).

Conduits narrower than 1 m are difficult to model, since the numerical calculation becomes instable. Our approach assumes a continuous upward flux of material. The result of the simulation is a velocity/diameter relation and hence a volume of material at the upper outflow with respect to channel width. We find that the velocity of upward migration changes by five orders of magnitude (Fig. 10a). In contrast to the velocity, the volume of mass outflow is in the same range of magnitude, varying from 10,000–30,000 m^3/yr (Fig. 10b). The total amount of conveyed thermal energy, connected to the mass flow is $0.5–1 * 10^3$ GJ/yr (Fig. 10c). The volume of mud appears to be remarkably indifferent to the width of the conduit and should be at least 10,000 m^3/yr to deliver mud of the observed temperature. The controlling factor for this is the heat flux through the shell of the conduit because the material loses 135 °C of its original temperature or 83% of its thermal energy during its ascent. To consider a conduit as wide as HMMV itself is not necessary in order to maintain a considerable amount of warm mud and a conduit smaller than 1 m in diameter would result in dramatically increasing velocities (above 12 km/yr).

Table 4
Parameters for mud volume calculation

T_0=−0.8 °C
T_{3000}=162 °C
k=1.2 W/m K
ρ=1950 kg/m^3
ρ=2000 kg/m^3
H=3000 m
D=1–1200 m

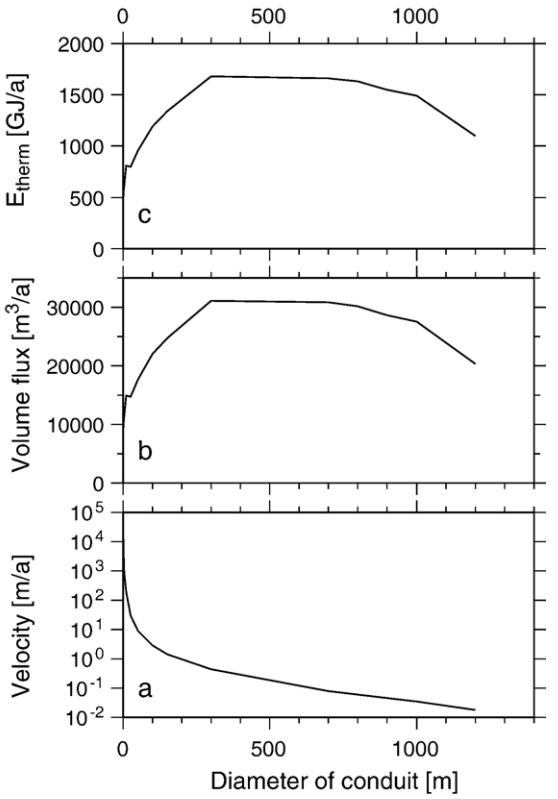

Fig. 10. Results of modeling rates of mud expulsion with respect to conduit diameter. Lower: migration velocity vs. conduit diameter. Boundary conditions are temperatures at lower and upper end of conduit. Middle: mud volume expulsion does not exceed certain limits. Upper: thermal energy, transported with the expulsed mud corresponds to the amount of mud.

5. Discussion

Temperature measurements in different depth ranges showed that none of the methods alone gives the entire picture of this thermally heterogeneous environment. Due to the limited position accuracy, estimated as ±30 m for each of the instruments, it was possible only at one site to combine data from three methods into a longer gradient. However, this is the key site at the most active center of HMMV and is used for subsequent modeling.

From the temperature measurements, we get three major insights: (1) the maximum temperature of material near the upper end of the conduit is about 26 °C, (2) very high vertical temperature gradients of 2000–3000 mK/m only occur near the surface and do not continue to greater depths and (3) there is a steep horizontal gradient in temperature at a distance of 300–500 m from the eruptive center.

These observations allow us to divide the measured temperature fields into two classes, one related to small scale surface effects and the other related to deep-seated and long-term effects.

Looking at the small scale effects, based on modeling, we interpret that we were able to observe a mud flow less than 3 days old. This corresponds to seafloor observations with ROV "Victor 6000", which show a homogeneous grey mud with absolutely no benthic bioactivity. Evaluating the high resolution bathymetry, this flow covers an area of 5000 m^2 while the height is estimated as 3–4 m. The latter value is derived from the bulge-like temperature distribution and additionally from the bathymetric mapping. A calculated mud volume of 15,000–20,000 m^2 is greater or equal to the total annual discharge of HMMV. Thus, we can estimate that a mud flow like the observed one occurs about once a year.

The second aspect is the deeper structure of HMMV and the root of its supply channel down to 3000 mbsf, which was numerically modeled. Two seismic sections (D2-82 and 7200-77 of Hjelstuen et al., 1999) show downward bent reflectors for a horizontal extent of 1.0–1.5 km underneath HMMV, exactly the size of the surfacial expression of HMMV. Hjelstuen et al. (1999) attributed this effect to a near surface velocity reduction. Horizontal resolution, expressed as the size of the first Fresnel zone, can be estimated as 500–700 m. A vertical channel of that size cannot be observed further downward. It is remarkable that the seismic expression of a vertical channel and the effective diameter of this channel differ greatly, as we have to consider that only small conduits are available for migration of mud and fluids within a broader chimney of mud breccia. A similar discussion is found in Krastel et al. (2003) for the Dvurechenskii Mud Volcano (Black Sea), where they can even trace seismic horizons through the apparent feeder channel. For low viscosity muds, effective pathways need not be wider than a few decimeters or meters, according to Poiseuille's and Stoke's laws and the observations compiled by Kopf and Behrman (2000).

Looking for a classification of HMMV in comparison to other mud volcano phenomena, we find that HMMV is a mud pie rather than a volcano as described for the Barbados accretionary prism (Henry et al., 1996). From analog modeling, it is known that there is a relationship between surface expression and width of the feeder (Lance et al., 1998). Mud pies indicate wide conduits, while mud domes result from narrow ones, using the same material. Wide conduits in this case mean diameters ranging from a few decimeters up to a few meters. Soft mud also means a high content of water within the transported material. As this material is a three-component substrate of mineral, water and gas, energy transport is predominantly coupled to the amount of water within the substrate because water is the most abundant component and specific heat capacity of water is four times that of the mineral components. The gaseous component is almost negligible with regard to energy transport.

The effect of rapid sedimentation cannot be neglected at this site. The crustal heat flow related to 33–37 Ma old crust should be 80 mW/m^2 according to the model of Parsons and Sclater (1977). It is convenient to consider only the glacial sedimentary unit because its sedimentation rate is more than 10 times that of the lower preglacial sequence. A mean rate of 1.35 mm/yr for 2.3 Ma results in a gradient reduction of 55% according to von Herzen and Uyeda (1963). We actually find values of around 52–65 mW/m^2 outside the crater of HMMV. This indicates a bias to higher heat flow than the expected 40 mW/m^2. Either an increased basal heat flow or a heat source within the terrigenous material of the glacial unit may be the cause of this bias. Thermal conductivity, increased by this magnitude, seems unrealistic.

In comparison to this feature, the much smaller structure "Mound 11" off the coast of Costa Rica shows an only slightly disturbed temperature field even though the mound is active in terms of gas hydrate generation and CH_4 degassing (Schmidt et al., 2005).

6. Summary and conclusion

Close investigation of the thermal structure of HMMV reveals the dynamic behavior of this active source of mud, fluid and gas. Narrow spaced temperature measurements allowed an upper temperature limit for outflow of mud to be constrained. Together with the temperature estimate for the deep-seated source of material, this enables the volume of mud convection to be modeled. Having the upper and lower temperatures as known parameters of the conduit, the result is a set of velocity/diameter values. The heat content of the system is balanced by the amount of heat, dissipating through the mantle surface of the conduit. The surprising result is that the transported volume is relatively indifferent, at a

rate of 10,000–30,000 m^3/yr for conduits larger than 1 m in diameter.

The detection of a mud flow only 3 days old is constrained by three features (a) its core temperature of ~ 26 °C, which can be anticipated to be the effluent temperature of the conduit, (b) the very steep gradient below the mud line, determined by the mini-lance and (c) the virtually unpopulated surface of the area, observed on ROV "Victor 6000" images. A process of successive mud flows cannot be the cause for the high temperatures of 20–23 °C below 10 mbsf because cooling of a singular mud layer would take only 3 months. Thus, mud flows at a frequency of one per year would cool to the ambient environment, before being superposed by a new one. Our conclusion is that only part of the conveyed heat reaches the surface while a substantial amount of energy and probably material is distributed at the bottom side of the mud pond. Cooling of this "underplated material" is achieved via conduction through the shell of the pond and by convection of fluids upwards. The upward migration of fluid and gas is proven by the evaluation of chemical and thermal gradients (de Beer et al., 2006). Furthermore, gas bubbles emerging from HMMV have been observed in significant volumes (Klages et al., 2004). HMMV has to be considered a three-phase system, where gas, water and sediment particles might have different behaviors during their uplift (de Beer et al., 2006).

The thermal situation of HMMV as a whole must have been stable for at least thousands of years. The thermal aurora, indicated by the horizontal gradient, integrates the source strength with respect to time and temperature. The long-term temperature of HMMV should be between 15 and 30 °C. Higher temperatures would yield higher than observed temperatures outside the pond.

Acknowledgements

Many thanks go to Kapitän Domke of *R/V Polarstern* and his crew for supplying excellent seamanship during ARK XIX/3b. We are grateful to the Alfred Wegener Institute, namely Michael Klages, Michael Schlüter and Antje Boetius, for finance and support of this project. We thank Jeffrey Poort and an unknown reviewer, who helped to improve the paper.

References

Camerlenghi, A., Cita, M.B., Hieke, W., Ricchiuto, T., 1992. Geological evidence for mud diapirism on the Mediterranean Ridge accretionary complex. Earth and Planetary Science Letters 109, 493–504.

Camerlenghi, A., Cita, M.B., Vedova, B.D., Fusi, N., Mirabile, L., Pellis, G., 1995. Geophysical evidence of mud diapirism on the Mediterranean Ridge accretionary complex. Marine Geophysical Researches 17, 115–141.

Cita, M.B., Woodside, J.M., Ivanov, M.K., Kidd, R.B., Limonov, A.F., Scientific Staff of Cruise TTR3-Leg 2, 1994. Fluid venting, mud volcanoes and mud diapirs on the Mediterranean Ridge. Accademia Nazionale dei Lincei, Rendiconti Classe di Scienze Fisiche, Matematiche e Naturali 9 (5), 159–169.

Crane, K., Sundvor, E., Foucher, J.-P., Hobart, M., Myhre, A.M., LeDouran, S., 1988. Thermal evolution of the Western Svalbard Margin. Marine Geophysical Research 9, 165–194.

de Beer, D.E., Sauter, H., Niemann, N., Kaul, J.-P., Foucher, U., Witte, M., Schlüter, A., Boetius, 2006. In situ fluxes of microbial activity in surface sediments of the Håkon Mosby Mud Volcano. Limnology and Oceanography 51 (3).

Eldholm, O., Sundvor, E., Vogt, P.R., Hjelstuen, B.O., Crane, K., Nilsen, A.K., Gladczenko, T.P., 1999. SW Barents Sea continental margin heat flow and Håkon Mosby Volcano. Geo-Marine Letters 19, 29–37.

Fiedler, A., Faleide, J.I., 1996. Cenocoic sedimentation along the south-western Barents Sea margin in relation to erosion and uplift of the shelf. Global and Planetary Change 12, 75–93.

Géli, L., Turon, J.-L., Aslanian, D., Balut, Y., Beuzart, P., Cochran, J., Francheteau, J., Harmegnies, F., Landuré, J.-Y., et al., 2001. Deep-penetration heat flow probes raise questions about interpretation from shorter probes. EOS 82, 317–320.

Ginsburg, G.D., Milkov, A.V., Soloviev, A.V., Egorov, A.V., Cherkashev, G.A., Vogt, P.R., Crane, K., Lorenson, T.D., Khutorskoy, M.D., 1999. Gas hydrate accumulation at the Håkon Mosby Mud Volcano. Geo-Marine Letters 19, 57–67.

Henry, P., LePichon, X., Lallemant, S., Lance, S., Martin, J.B., Foucher, J.P., Fiala-Médioni, A., Rostek, F., Guilhaumou, N., et al., 1996. Fluid flow in and around a mud volcano field seaward of the Barbados accretionary wedge: results from Manon cruise. Journal of Geophysical Researches 101, 20297–20323.

Hjelstuen, B.O., Eldholm, O., Faleide, J.I., Vogt, P.R., 1999. Regional setting of Håkon Mosby Mud Volcano, SW Barents Sea margin. Geo-Marine Letters 19, 22–28.

Hyndman, R.D., Davis, E.E., Wright, J.A., 1979. The measurement of marine geothermal heat flow by a multipenetration probe with digital acoustic telemetry and in situ thermal conductivity. Marine Geophysical Researches 4, 181–205.

Klages, M., Thiede, J., Foucher, J.-P., 2004. The expeditions ARK XIX 3a, 3b and 3c. Berichte zur Polarforschung, p. 488.

Kopf, A.J., 2002. Significance of mud volcanism. Reviews Geophysics 40 (2), 1005.

Kopf, A.J., Behrman, J.H., 2000. Extrusion dynamics of mud volcanoes on the Mediterranean Ridge accretionary complex. In: Venderville, B., Mart, Y., Vigneresse, J.-L. (Eds.), From the Arctic to the Mediterranean: Salt, Shale, and Igneous Diapirs in and Around Europe. Geol. Soc. London, London, pp. 169–204.

Krastel, S., Spiess, V., Ivanov, M., Weinrebe, W., Bohrmann, G., Shashkin, P., Heidersdorf, F., 2003. Acoustic investigations of mud volcanoes in the Sorokin Trough, Black Sea. Geo-Marine Letters 23, 230–238.

Lance, S., Henry, P., Le Pichon, X., Lallemant, S., Chamley, H., Rostek, F., Faugeres, J.-C., Gonthier, E., Olu, K., 1998. Submersible study of mud volcanoes seaward of Barbados accretionary wedge: sedimentology, structure and rheology. Marine Geology 145, 255–292.

Müller, R.D., 1997. Digital isochrones of the world's ocean floor. Journal of Geophysical Research 102, 3211.

National Geophysical Data Center, 2004. Global Digital Elevation Model (ETOPO2), ESRI, Redlands, California, USA.

Parsons, B., Sclater, J.G., 1977. An analysis of the variation of ocean floor bathymetry and heat flow with age. Journal of Geophysical Research 32, 803–827.

Schmidt, M., Hensen, C., Mörz, T., Müller, C., Grevemeyer, I., Wallmann, K., Mau, S., Kaul, N., 2005. Methane hydrate accumulation in "Mound 11" Mud Volcano, Costa Rica fore arc. Marine Geology 216, 77–94.

Sundvor, E., Eldholm, O., Gladczenko, T.P., Planke, S., 2000. Norwegian–Greenland Sea thermal field. Geological Society of London Special Publication 167, 397–410.

Vogt, P.R., Cherkashev, G., Ginsburg, G., Ivanov, G., Milkov, A., Crane, K., Lein, A., Sundvor, E., Pimenov, N., Egorov, A., 1997. Håkon Mosby Mud Volcano provides unusual example of venting. EOS, Transactions, AGU 78, 549–557.

Vogt, P.R., Gardner, J., Crane, K., 1999. The Norwegian–Barents–Svalbard (NBS) continental margin: introducing a natural laboratory of mass wasting, hydrates, and ascent of sediment, pore water, and methane. Geo-Marine Letters 19, 2–21.

von Herzen, R., Uyeda, S., 1963. Heat flow through the east Pacific Ocean floor. JGR 4219–4250.